Remote Sensing of Environment 221 (2019) 363–372

Contents lists available at ScienceDirect

Remote Sensing of Environment

journal homepage: www.elsevier.com/locate/rse

Evaluation of SMAP downscaled brightness temperature using SMAPEx-4/5 airborne observations

N. Ye[a,*], J.P. Walker[a], R. Bindlish[b], J. Chaubell[c], N.N. Das[c], A.I. Gevaert[d], T.J. Jackson[e], C. Rüdiger[a]

[a] Department of Civil Engineering, Monash University, Australia
[b] NASA Godard Space Flight Center, United States
[c] NASA Jet Propulsion Laboratory, United States
[d] Department of Earth Sci-ences, Earth and Climate Cluster, VU University Amsterdam, the Netherlands
[e] The U. S. Department of Agriculture, United States

ARTICLE INFO

Keywords:
SMAP
Downscaled brightness temperature
Validation
Field experiment

ABSTRACT

The Soil Moisture Active and Passive (SMAP) mission, launched by the National Aeronautics and Space Administration (NASA) on 31st January 2015, was designed to provide global soil moisture every 2 to 3 days at 9 km resolution by downscaling SMAP passive microwave observations obtained at 36 km resolution using active microwave observations at 3 km resolution, and then retrieving soil moisture from the resulting 9 km brightness temperature product. This study evaluated the SMAP Active/Passive (AP) downscaling algorithm together with other resolution enhancement techniques. Airborne passive microwave observations acquired at 1 km resolution over the Murrumbidgee River catchment in south-eastern Australia during the fourth and fifth Soil Moisture Active Passive Experiments (SMAPEx-4/5) were used as reference data. The SMAPEx-4/5 data were collected in May and September 2015, respectively, and aggregated to 9 km for direct comparison with a number of available resolution-enhanced brightness temperature estimates. The results show that the SMAP AP downscaled brightness temperature had a correlation coefficient (R) of 0.84 and Root-Mean-Squared Error (RMSE) of ~10 K, while SMAP Enhanced, Nearest Neighbour, Weighted Average, and the Smoothing Filter-based Modulation (SFIM) brightness temperature estimates had somewhat better performance (RMSEs of ~7 K and an R exceeding 0.9). Although the SFIM had the lowest unbiased RMSE of ~6 K, the effect of cloud cover on Ka-band observations limits data availability.

1. Introduction

Soil moisture is a key variable at the interface between the atmosphere and the land surface, affecting global water, energy, and carbon cycles (Falloon et al., 2011; Jung et al., 2010; Seneviratne et al., 2010). Information on its temporal and spatial distribution is required for a variety of disciplines including hydrology, meteorology, climate, and agriculture (Crow et al., 2012; Ryu and Famiglietti, 2006; Sellers et al., 1997). Due to its all-weather capability, direct relationship with volumetric soil moisture content, and reduced impacts from vegetation and surface roughness, passive microwave remote sensing techniques have been widely acknowledged as the most promising approach to measure near surface soil moisture (Ulaby et al., 1981). Therefore, the first space mission dedicated to global soil moisture monitoring was launched on 2nd November 2009; the Soil Moisture and Ocean Salinity (SMOS) satellite, operated by the European Space Agency, carries an L-band (1.41 GHz) microwave radiometer to observe volumetric soil water content of the top 5 cm with a spatial resolution of 40 km (Kerr et al., 2010). However, to satisfy the spatial resolution requirement of better than 10 km for hydrometeorological applications (Crow et al., 2005; Entekhabi et al., 1999), a number of algorithms have been proposed to downscale the microwave radiometer observations using ancillary optical or radar data with a higher resolution (Peng et al., 2017; Sabaghy et al., 2018). Subsequently, the downscaled radiometer observations can be used to retrieve soil moisture with improved spatial resolutions using radiative transfer models (de Rosnay et al., 2009; Mo et al., 1982; Wigneron et al., 2007). As an innovative solution, the Soil Moisture Active Passive (SMAP) mission, launched by the National Aeronautics and Space Administration (NASA) on 31st January 2015, was designed to estimate global soil moisture with a resolution of 9 km using a

* Corresponding author.
E-mail address: nan.ye@monash.edu (N. Ye).

https://doi.org/10.1016/j.rse.2018.11.033
Received 15 March 2018; Received in revised form 10 November 2018; Accepted 22 November 2018
Available online 28 November 2018

combined L-band (1.41 GHz) radiometer and L-band (1.26 GHz) radar (Entekhabi et al., 2010). SMAP uses a conically scanning mesh antenna to provide oversampled brightness temperatures in 3-dB elliptical footprints of 39 km by 47 km with a spacing of 11 km along scans and 31 km across scans. The SMAP radiometer brightness temperature observations are resampled onto a 36 km grid and downscaled to 9 km by merging them with 3 km radar backscatter observations acquired simultaneously. This was possible until the failure of the SMAP radar on 7th July 2015. As a consequence of this failure, a number of alternative resolution enhancement algorithms have been considered to downscale the SMAP radiometer observations (and/or retrieved soil moisture). The objective of this paper is to evaluate their performance using airborne radiometer observations collected during the SMAPEx-4/5 field experiments. It needs to be noted that SMAPEx-4 was the only extensive airborne field experiment accomplished world-wide prior to the malfunction of the SMAP radar, making it a unique data set for validating the SMAP Active/Passive downscaling algorithm.

2. Study area

The Soil Moisture Active Passive Experiments (SMAPEx) are a series of five airborne field campaigns across different seasons conducted over a six year timeframe (2010 to 2015) (Panciera et al., 2014; Ye et al. submitted). The fourth and fifth SMAPEx experiments (SMAPEx-4/5) took place at the beginning of the SMAP operational phase in May and September 2015, respectively, to provide extensive airborne and ground sampling data for the SMAP in-orbit validation (Ye et al. submitted). Airborne radar and radiometer observations were collected over the same frequencies as the SMAP instruments and timed to coincide with the regular SMAP overpasses.

The SMAPEx-4/5 experiments were conducted in the Yanco area of the Murrumbidgee River catchment in south-eastern Australia (Fig. 1). This SMAP core validation site (Colliander et al., 2017) is dominated by flat cropping and grazing lands. An area in size of 71 km × 89 km (containing at least a complete 3-dB footprint of the SMAP radiometer in each orbit) was designed for the SMAP validation flights. Additionally, an area of 95 km × 116 km (containing a 3-dB footprint of Beam 2 of the Aquarius radiometer on 11th May 2015) was included during SMAPEx-4. Due to the failure of Aquarius on 7th June 2015, only the SMAP validation flight area was sampled during SMAPEx-5. Consequently, only data over the SMAP validation flight area were compared in this study.

During SMAPEx-4, the main land surface types were bare soil in cropping areas and short grass across the grazing areas. Soil moisture conditions started at ~0.1 m^3/m^3 with an average vegetation water content of ~0.1 kg/m^2, followed by rainfall events on 9th and 18th May, resulting in heterogeneous soil moisture scenarios for the SMAP downscaling validation under low vegetation conditions. The SMAPEx-5 campaign started after a series of extensive rainfall events with no further rainfall during the campaign. This provided an ideal dry-down period, resulting in a wide range of soil moisture scenarios. In addition, the main vegetation types were wheat in the cropping areas and dense grasses in the grazing areas. The vegetation water content was higher than during SMAPEx-4 (up to ~2 kg/m^2) and had a strong variation across the campaign period due to high growth rates during the Austral spring.

3. Data sets

In the literature, a number of algorithms have been developed for SMAP data downscaling, and can be categorized into three classes: i) radar-downscaled; ii) radiometer-only; and iii) optical/radiometer-downscaled. The SMAP mission was designed to downscale 36 km radiometer observations using its own on-board L-band radar. The active/passive concept was the main SMAP downscaling approach until the failure of the SMAP radar. Subsequently, Das et al. (2016) proposed an alternative radar downscaling approach using the Sentinel C-band radar observations (Rüdiger et al., 2016; Torres et al., 2012). Moreover, as the SMAP radiometer conically scans the ground with a 3-dB elliptical footprint of 39 km by 47 km every 11 km along scan circles and every 31 km between scan circles, several radiometer-only algorithms have been proposed for directly interpolating the oversampled SMAP radiometer observations to 9 km resolution using different posting approaches: nearest neighbour, weighted average, and deconvolution (Backus and Gilbert, 1970; Chan et al., 2018; Dumedah et al., 2014; Entekhabi et al., 2010; Gevaert et al., 2016). Alternative approaches include the use of high resolution optical and radiometer observations to downscale SMAP radiometer observations to 1 km resolution (Gevaert et al., 2016). However, the availability of optical and high frequency radiometer is adversely influenced by cloud cover and intense precipitation, which in turn limits the application of optical/radiometer downscaling algorithms.

In this study, the five brightness temperature downscaling algorithms listed in Table 1 were evaluated, using the SMAPEx airborne observations as the independent reference. The following sub-sections describe the details of the respective products. Among them, SMAP Active/Passive and SMAP Enhanced products can be freely downloaded from the NASA EarthData website (https://earthdata.nasa.gov), the other data sets need to be requested from the authors. It should also be noted that the Sentinel radar downscaling algorithm could not be evaluated in this study due to there being no Sentinel-1 coverage coincident with SMAP overpasses during the periods of SMAPEx-4.

A. *SMAPEx*

The SMAPEx brightness temperature observations were collected using the Polarimetric L-Band Multi-beam Radiometer (PLMR) which provides dual-polarized (horizontally and vertically) brightness temperature observations at L-band (1.41 GHz) from six beams at incidence angles of 7°, 21.5° and 38.5° on both sides of the flight track. At the flight altitude of ~3000 m above the ground, airborne PLMR brightness temperature observations at 1 km resolution were collected between 3 am and 9 am (local time), being centred on the nominal SMAP descending/morning overpass time; it was found from calculations using ground monitoring station data that the near surface soil brightness temperature varied by only ~1 K during the individual flights, due to minimal variations of the effective soil temperature during the morning. The acquired PLMR observations were normalized to the incidence angle of the outer beams (38.5°) following the approach of Ye et al. (2015), and thermally corrected to the SMAP nominal overpass time of 6 am using a polynomial regression approach. Before and after each flight, the calibration of PLMR was confirmed by using the sky as a cold target and microwave absorber as a warm target. An accuracy of better than 1.4 K was found for both horizontal and vertical polarizations throughout SMAPEx-4/5. However, a bias of −2.4 K and correlation coefficient of 0.97 was observed when comparing PLMR brightness temperature observations and SMAP radiometer L1C data at 36 km scale (Ye et al. submitted). Consequently, for the purpose of evaluating the five SMAP downscaled brightness temperature approaches listed above, this bias was removed from all PLMR brightness temperature observations prior to their use as an independent reference in this study. The characteristics of SMAPEx PLMR brightness temperature observations and SMAP downscaled brightness temperature estimates are summarized in Table 1.

B. *SMAP AP*

The SMAP Active/Passive (AP) downscaled brightness temperature product was planned to be a key SMAP standard product with 9 km resolution (Entekhabi et al., 2010). A linear relationship between changes in radiometer brightness temperature and changes in radar backscatter, derived from time-series radar and radiometer

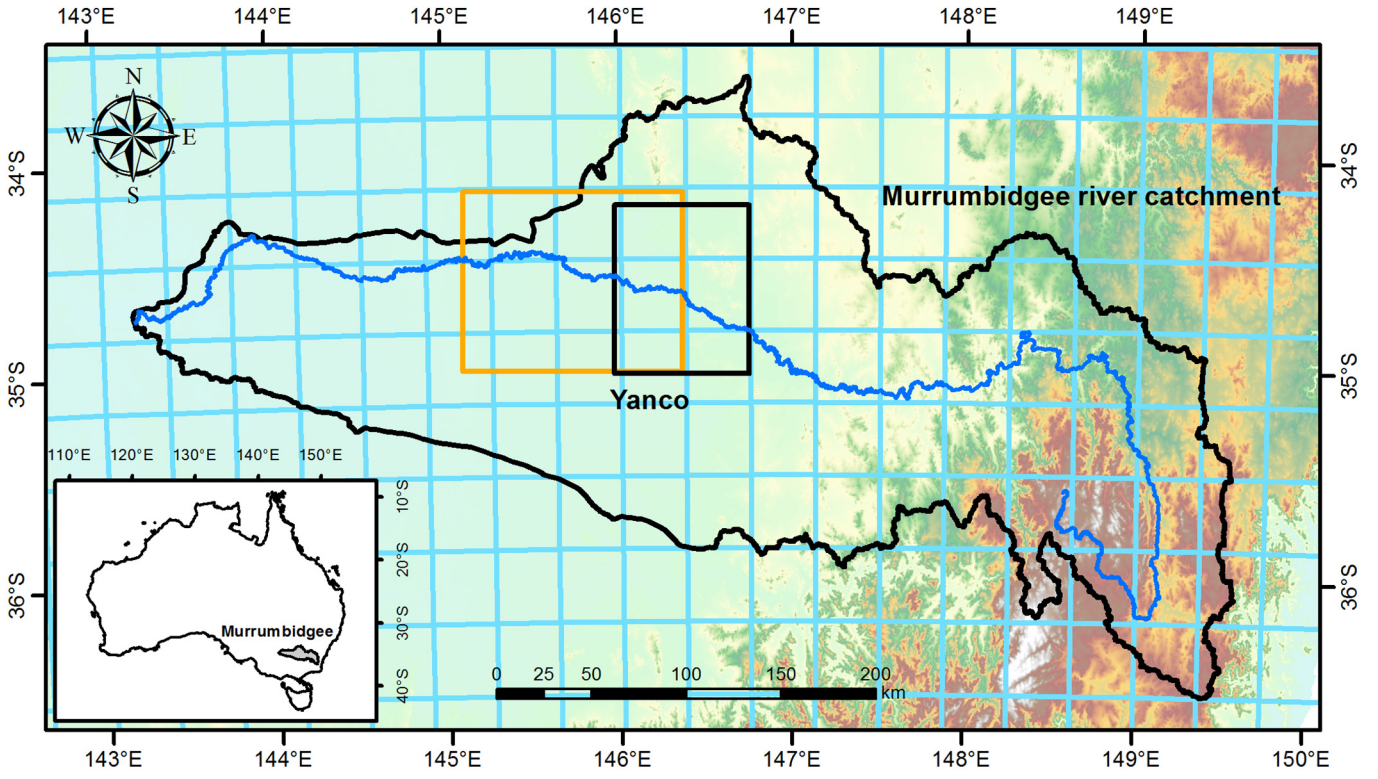

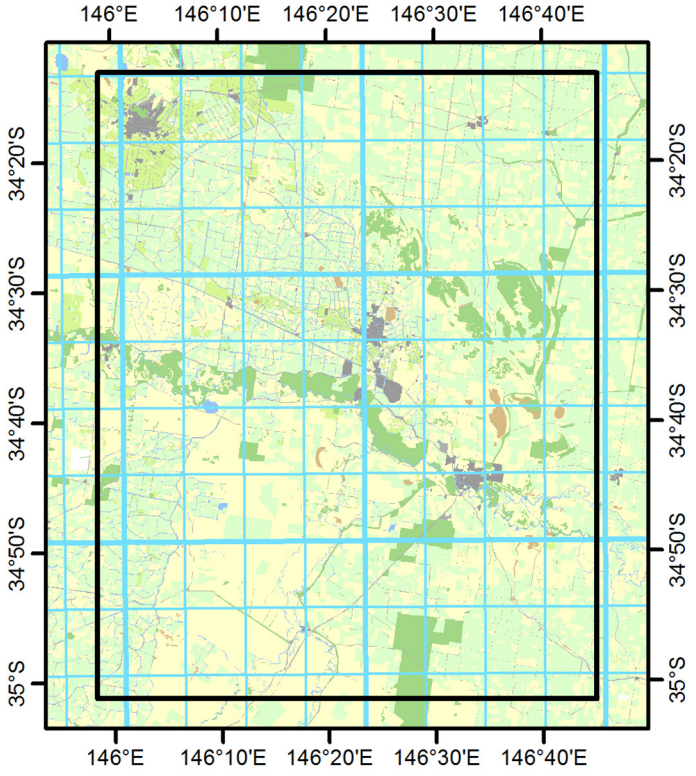

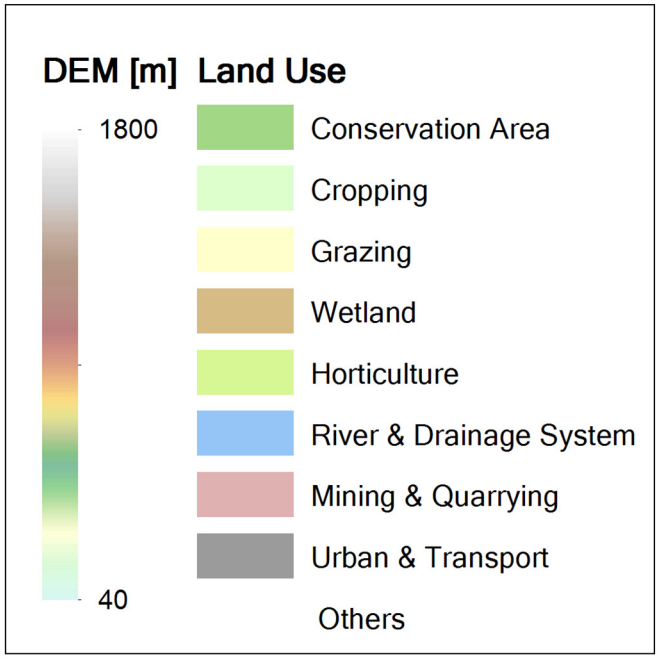

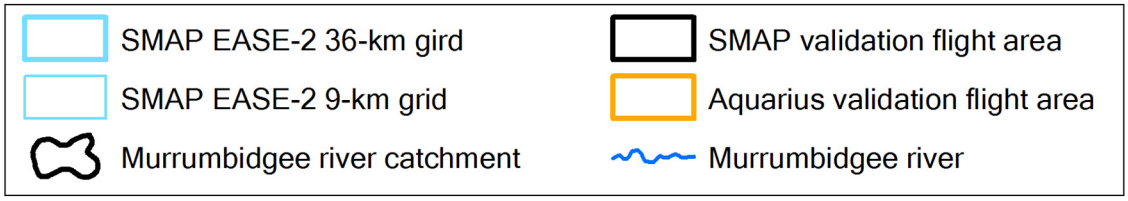

(caption on next page)

Fig. 1. Location of the SMAPEx-4/5 flight areas in the Murrumbidgee River catchment overlain with the Digital Elevation Model (DEM) and the SMAP EASE-2 36-km grid (top panel); Location of the SMAP validation flight area overlain with the land use map and the SMAP EASE-2 grids at 9-km scales (bottom panel).

Table 1
Summary of SMAPEx observations and SMAP downscaled brightness temperature estimates.

Algorithm	Class	Source	Grid	Resolution
SMAPEx		PLMR	UTM S55	1 km
SMAP AP	Radar downscaled	SMAP radiometer & radar	EASE-2	9 km
SMAP enhanced	Radiometer only	SMAP radiometer	EASE-2	9 km
Nearest neighbour	Radiometer only	SMAP radiometer	EASE-2	9 km
Weighted average	Radiometer only	SMAP radiometer	EASE-2	9 km
SFIM	Optical/radiometer downscaled	SMAP radiometer &AMSR-2	WGS84	0.1°

measurements over each pixel, was used to disaggregate the 36-km brightness temperature observations using the 3-km backscatter observations (Entekhabi et al., 2014). In this study, the SMAP L2 SM AP product in version R11850 was used.

C. *SMAP Enhanced*

The SMAP Enhanced brightness temperature product (Backus and Gilbert, 1970; Chan et al., 2018) is an interpolation of the SMAP L1B brightness temperature onto the EASE-2 9-km grid using the Backus-Gilbert algorithm, which can estimate brightness temperatures on a regular grid with a higher posting resolution of 9 km (BG does not modify the original resolution of ~33 km) and a lower error from irregular sampling data (Chaubell, 2016). The interpolation, which fully accounts for the antenna pattern, is considered "optimal" in the sense that the interpolated value would be similar to the value obtained if the measurement had actually been taken. In this study, the SMAP L2 SM P E product in version R16010 was used.

D. *Nearest Neighbour*

According to a previous study on SMOS brightness temperatures (Dumedah et al., 2014), oversampled coarse resolution passive microwave data can be posted onto a higher resolution grid using the nearest neighbour approach, and result in a reasonable level of error (4.5 K for horizontal polarization and 3.9 K for vertical polarization) compared with airborne brightness temperature observations as truth. In this approach, the centre part of the SMAP 3-dB footprint was assumed to contribute most of the signal observed by the SMAP radiometer. The SMAP L1B brightness temperature data (version R16010) in both fore- and aft-ward looking directions were resampled together onto the SMAP EASE-2 9-km grid using the nearest neighbour approach for evaluation in this study.

E. *Weighted Average*

The SMAP L1B brightness temperature data are averaged to the SMAP EASE-2 9-km grid weighted by their antenna gain patterns within the given pixel. In this study, the Weighted Average data in fore- and aft-ward looking directions were averaged before comparison with SMAPEx data.

F. *Smoothing Filter-based Modulation (SFIM)*

The Smoothing Filter-based Modulation (SFIM) technique (Liu, 2000) was used to sharpen the coarse resolution SMAP radiometer brightness temperature data using higher resolution Ka-band brightness temperatures collected from the Advanced Microwave Scanning Radiometer 2 (AMSR2) (Gevaert et al., 2016). The higher resolution AMSR2 Ka-band brightness temperatures were aggregated to the lower resolution of the SMAP L1C brightness temperatures using a low pass filter. The ratio between the high and low resolution Ka-band brightness temperatures was then used to modulate the low-resolution SMAP brightness temperatures. The downscaled brightness temperatures were gridded onto 0.1° grid in the geographic WGS84 system, using a linear interpolation approach. In this study, the SFIM downscaling was performed only for days with SMAP descending (morning) and AMSR2 descending (night) overpasses available within a 6-hour interval. Due to the atmospheric effects of intense precipitation events at Ka-band, the SFIM downscaling is only applicable over the areas without intense precipitation.

4. Results and discussion

During SMAPEx-4/5, a total of 16 flights were conducted, with two of them not coinciding with a SMAP data acquisition due to problems of the SMAP star tracker and data downlink, respectively. The observed PLMR brightness temperature data at 1 km resolution was averaged to the grid of each SMAP downscaled brightness temperature estimate and compared with those brightness temperature values. As discussed above, it is worth noting that limiting the flight interval to 6-h in the early morning minimized surface soil temperature variations, which in turn limited the impact of temporal variation in the airborne brightness temperature observations. Figs. 2 and 3 show the horizontally polarized brightness temperature maps of averaged SMAPEx data on the EASE-2 9-km grid together with the SMAP downscaled brightness temperature estimates. As expected, vertically polarized brightness temperatures (not shown) had a similar spatial pattern to the horizontally polarized brightness temperature, but with a different range. Generally, all of the downscaled SMAP brightness temperature estimates had a similar temporal variation to the SMAPEx airborne data during the entire periods of SMAPEx-4/5, including the rainfall events on 9th and 18th May 2015. The SMAP Enhanced, Nearest Neighbour, Weighted Average, and SFIM brightness temperature estimates have similar and smoothed spatial distributions. Although local variability has been reduced, these brightness temperatures can still reflect the distribution pattern caused by the rainfall event on 18th May 2015. In contrast, the SMAP AP product had significant noise-like heterogeneity which may be attributed to the unaccounted spatial variation in surface roughness and "noisy" radar backscatter signal used in the downscaling.

In order to assess their performance, the SMAP downscaled brightness temperature estimates were compared with the averaged SMAPEx data at pixel level (Fig. 4). In addition, Root-Mean-Squared Error (RMSE) and correlation coefficient (R) between SMAP downscaled brightness temperature estimates and PLMR brightness temperature observations were calculated (see Figs. 5 and 6 respectively). All SMAP downscaled brightness temperature estimates have a good correlation to PLMR observations across the full range of observed brightness temperatures over the study area. However, a horizontal cluster pattern can be found in the SMAP Enhanced, Nearest Neighbour

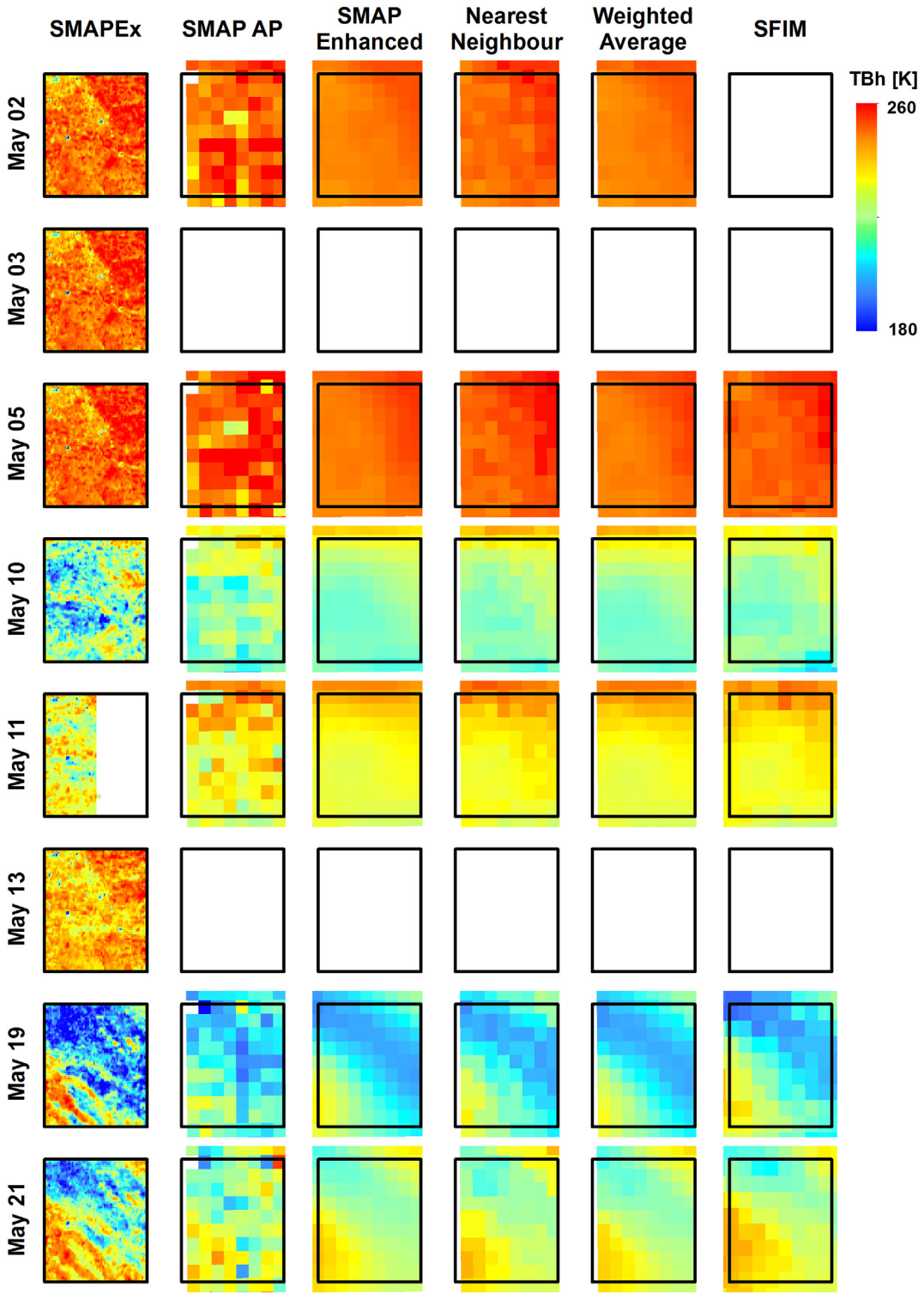

Fig. 2. SMAPEx PLMR observed and SMAP downscaled brightness temperature observations in horizontal polarization (TBh) over the SMAP validation flight area (black box) during SMAPEx-4.

and Weighted Average brightness temperature estimates, which were resampled from the SMAP 36-km radiometer observations alone. As expected, the nested 9-km pixels interpolated from the same 36-km pixel had a similar brightness temperature to the 36-km pixel with very limited variation when compared with the natural variability of SMAPEx data.

Moran's I spatial autocorrelation statistic (Moran, 1950) was also calculated for each sampling day and product, in order to investigate the temporal variation of spatial correlation between SMAPEx observations and the SMAP downscaled brightness temperature products. Given the small number of 9-km pixels over the study area, the weight factor in Moran's I function was simply defined as 1 for neighbouring pixels and 0 otherwise. Fig. 7 shows the time series of spatial autocorrelation of SMAP downscaled brightness temperature products and averaged SMAPEx brightness temperature on the SMAP 9-km EASE-2 grid. It needs to be noted that SMAPEx brightness temperature on 11th

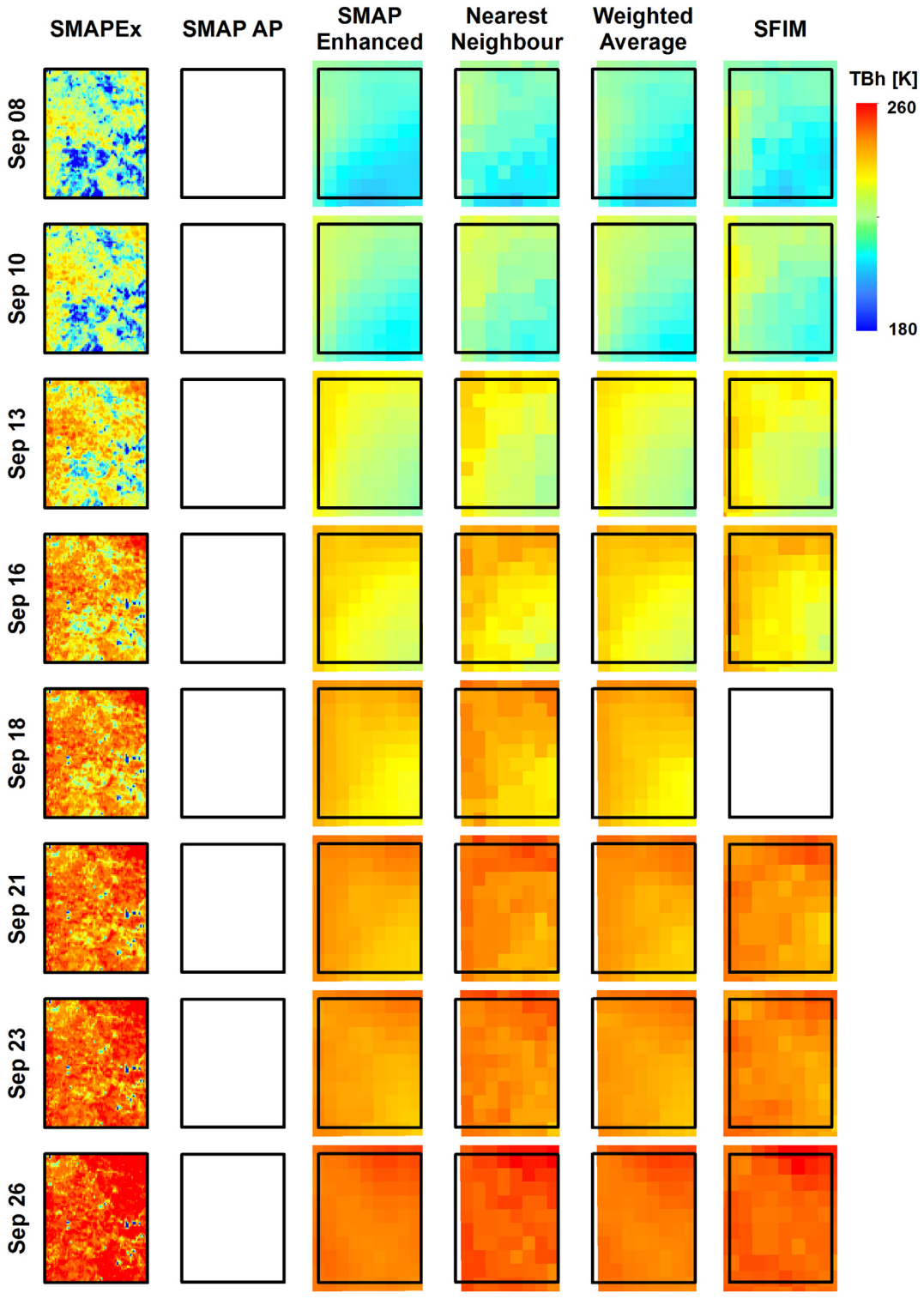

Fig. 3. Same as Fig. 2 except for SMAPEx-5.

May only covered a half of the SMAP validation flight area, resulting in a sudden decrease in Moran's I statistics. It can be found from Fig. 7 that the SMAP Enhanced and Weighted Average products had similar temporal variation and highest spatial correlation and that the SMAP AP product showed the lowest values. Taking the SMAPEx dataset as the reference, it implies that the spatial heterogeneity in SMAP Enhanced and Weighted Average products was significantly smeared, while additional noise from radar data was introduced in the SMAP AP product. Although the Nearest Neighbour and SFIM products had slightly better local spatial heterogeneity than the SMAP Enhanced and Weighted Average products, their considerable polarization differences and temporal trends of spatial correlation did not match those of SMAPEx. In contrast, the SMAP Enhanced and Weighted Average products had similar spatial correlation between horizontal and vertical polarizations.

Taking the averaged SMAPEx brightness temperature observations as an independent reference, the bias, correlation coefficient (R), Root-Mean-Squared Error (RMSE), and unbiased RMSE (ubRMSE) were

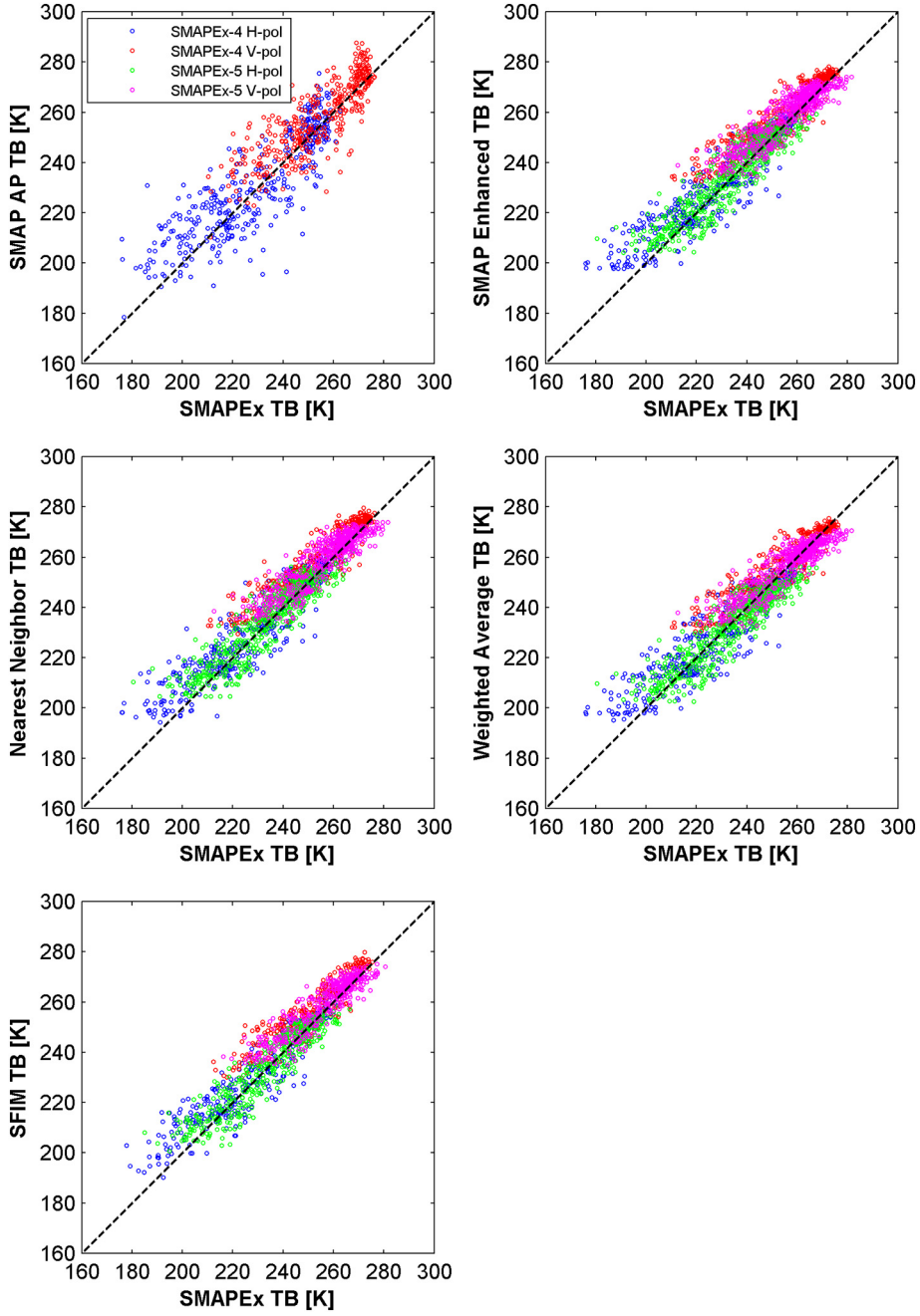

Fig. 4. Comparison between SMAP downscaled products and PLMR brightness temperature observations collected during SMAPEx-4/5.

calculated for each brightness temperature estimate (Table 2). According to the statistics, all the SMAP downscaled brightness temperature estimates had a lower R and higher RMSE under the heterogeneous conditions of SMAPEx-4 than the more homogeneous conditions of SMAPEx-5. An R better than 0.9 was achieved for all SMAP downscaled brightness temperature estimates except for SMAP AP (0.85). Similarly, SMAP AP had the highest RMSE of 11.64 K in horizontal polarization and 9.74 K in vertical polarization. Although SFIM had the highest bias in vertical polarization, its ubRMSEs in both polarizations were lower than other brightness temperature estimates. Compared to the horizontally polarized brightness temperature, the vertically polarized brightness temperature had a lower ubRMSE in all products, implying that it has a lower sensitivity to soil moisture. In addition, the vertically polarized brightness temperature had a higher bias in most of products. However, this might be a site-specific artefact and more experiments are required to identify the reasons behind this result.

According to evaluation results, the SMAP AP algorithm in the radar downscaling class had the poorest performance, as the SMAP radar added considerable noise to the downscaled brightness temperatures compared to radiometer-only downscaling products. The three radiometer-only downscaling algorithms had good and almost identical performance, since they were interpolated from SMAP L1B brightness temperature observations using different posting approaches. Under homogeneous conditions, different downscaled brightness temperatures methods in the radiometer-only class yielded similar values to the original SMAP radiometer observations. While the SMAP Enhanced and Weighted Average downscaling algorithms were able to improve the resolution of the SMAP radiometer observations, they also displayed a smoothed spatial pattern. Although the Nearest Neighbour was able to retain some local heterogeneity, its arbitrary assumption that the radiometer observation is mainly determined by the centre part of the

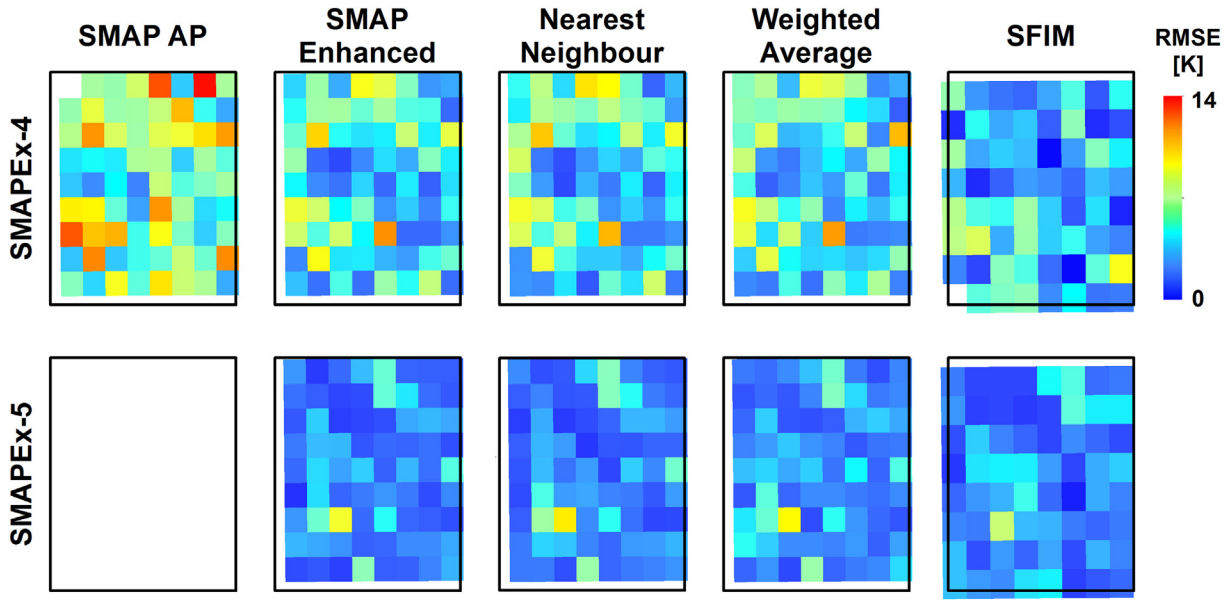

Fig. 5. Spatial maps of temporal RMSE between SMAP downscaled brightness temperature estimates and PLMR brightness temperature observations in horizontal polarization over the SMAP validation flight area (black box) during SMAPEx-4/5.

footprint can induce considerable error over areas with significant levels of heterogeneity, such as coasts, where parts of the footprint might impact on the overall observed brightness temperature. The SFIM algorithm in the optical/radiometer downscaled class had the best performance with slightly better RMSE and ubRMSE than the radiometer-only class. However, being similar to other optical/radiometer downscaling approaches, the SFIM downscaled products can be affected by cloud and/or intense precipitation.

In practice, the radiometer-only class can provide SMAP downscaling under all-weather conditions and without the need for input from other satellites. In particular, the SMAP Enhanced product is suggested due to its public availability, professional quality control, and capability of working over very heterogeneous areas. Based on the limited results from SMAPEx-4, the unique dataset obtained when the SMAP radar was operational, it can be concluded that the SMAP AP algorithm can be replaced with other downscaling algorithms, such as the SMAP Enhanced downscaling algorithms, for providing adequate global 9-km resolution brightness temperature products. The performance of other radar downscaling algorithms, such as Sentinel-1 downscaling algorithms, still needs to be further investigated.

5. Conclusions

The SMAP satellite, launched on 31st January 2015, aimed at providing global soil moisture with an unprecedented resolution of 9 km by downscaling 36-km radiometer brightness temperature observations using coincident 3-km radar backscatter observations. However, due to the failure of the on-board radar a number of alternative algorithms were proposed to downscale the SMAP radiometer observations. This study evaluated the currently available SMAP downscaled brightness

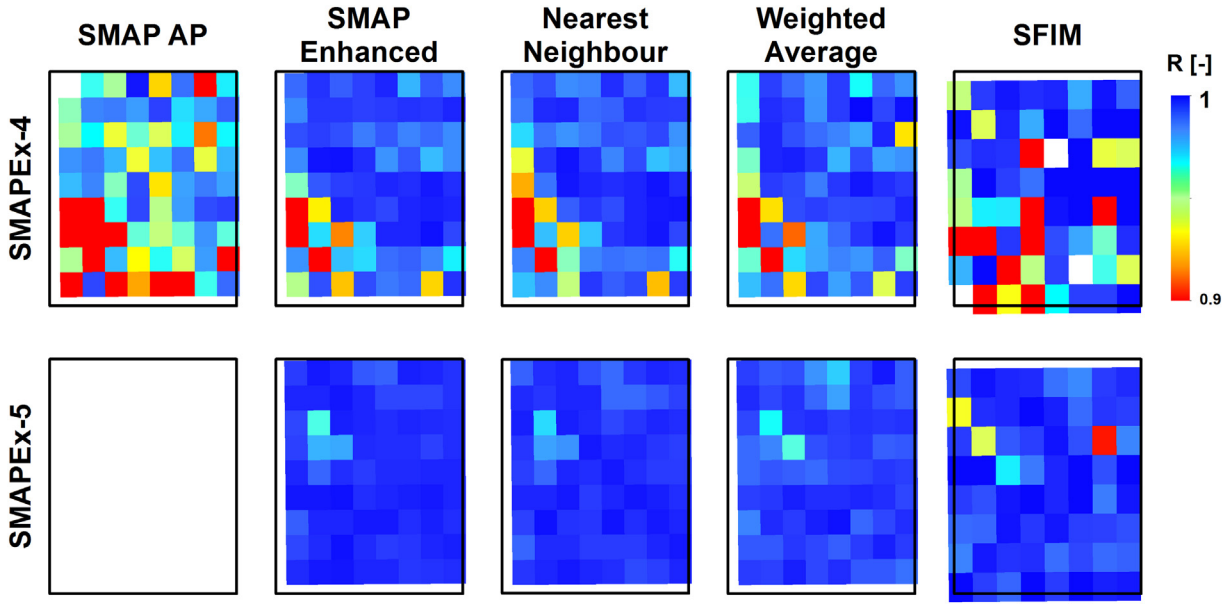

Fig. 6. Spatial maps of temporal correlation coefficient (R) between SMAP downscaled brightness temperature estimates and PLMR brightness temperature observations in horizontal polarization over the SMAP validation flight area (black box) during SMAPEx-4/5.

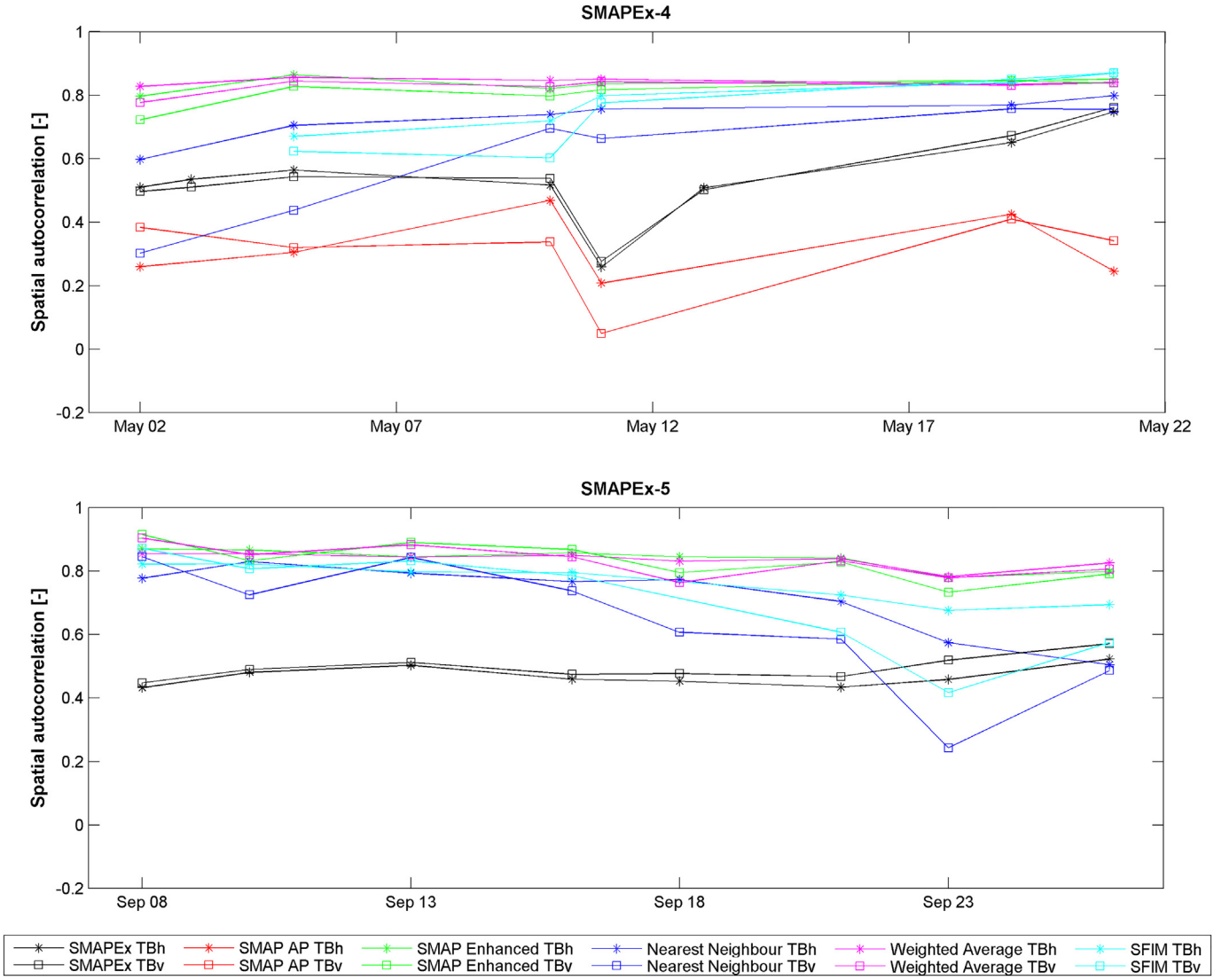

Fig. 7. Time series of spatial autocorrelation (Moran's I) of PLMR and SMAP downscaled brightness temperature maps in horizontal and vertical polarization during SMAPEx-4 (top) and −5 (bottom).

Table 2
Statistics of horizontally (vertically) polarized brightness temperature comparison between averaged airborne brightness temperature observations and SMAP downscaled estimates, including Bias, correlation coefficient (R), Root-Mean-Squared Error (RMSE), and unbiased RMSE (ubRMSE) for SMAPEx-4 and -5 (top and bottom lines respectively).

SMAPEx-4 SMAPEx-5	Bias [K]	R [−]	RMSE [K]	ubRMSE [K]
SMAP AP	2.40(4.15)	0.85(0.84)	11.64(9.74)	11.39(8.81)
	-	-	-	-
SMAP enhanced	3.31(5.63)	0.93(0.93)	8.68(8.40)	8.02(6.24)
	1.18(3.04)	0.92(0.90)	6.32(6.29)	6.21(5.50)
Nearest neighbour	3.24(5.62)	0.93(0.93)	8.71(8.37)	8.08(6.20)
	1.06(2.98)	0.92(0.90)	6.45(6.36)	6.36(5.62)
Weighted average	1.32(3.42)	0.92(0.92)	8.53(7.37)	8.43(6.52)
	-1.20(0.62)	0.92(0.90)	6.48(5.70)	6.36(5.66)
SFIM	2.77(6.39)	0.93(0.92)	8.09(8.70)	7.60(5.90)
	0.26(3.20)	0.94(0.91)	5.86(6.23)	5.86(5.35)

temperature estimates over the study area for the periods of SMAPEx-4/5, using airborne brightness temperature observations collected from the SMAPEx airborne field experiments as an independent reference. The comparison indicated that all SMAP downscaled brightness temperatures had higher correlation and lower RMSE when compared to airborne passive microwave observations in the more homogeneous scenarios during SMAPEx-5. The SMAP AP product was found to have the lowest correlation coefficient of 0.84 and highest RMSE of 11.64 and 9.74 K for horizontal and vertical polarizations respectively. The other SMAP downscaled brightness temperatures had a RMSE of ~7 K and a correlation coefficient of better than 0.9. Although the SFIM method can be adversely affected by intense precipitation, its unbiased RMSE of ~6 K was slightly lower than others. The SMAP Enhanced, Nearest Neighbour and Weighted Average brightness temperature estimates derived from the SMAP radiometer observations alone using different interpolation techniques all had a similar performance, with an unbiased RMSE of ~7 K. It is therefore concluded that any of these approaches can be an acceptable alternative for downscaling the SMAP brightness temperature at 9-km resolution. The SMAP Enhanced downscaled product is suggested as a suitable replacement for the SMAP Active/Passive product for practical applications at ~9-km scales, due to its good performance, data availability, and reliability over heterogeneous areas.

Acknowledgements

This work was supported within the framework of the MoistureMonitor project funded by the Australian Research Council (DP140100572).

References

Backus, G., Gilbert, F., 1970. Uniqueness in the inversion of inaccurate gross earth data. Philos. Trans. R. Soc. London, Ser. A 266, 123–192.
Chan, S., Bindlish, R., O'Neill, P., Jackson, T., Njoku, E., Dunbar, S., Chaubell, J., Piepmeier, J., Yueh, S., Entekhabi, D., 2018. Development and assessment of the SMAP enhanced passive soil moisture product. Remote Sens. Environ. 204, 931–941.
Chaubell, J., 2016. Soil Moisture Active Passive (SMAP) Project Algorithm Theoretical Basis Document SMAP L1B Enhancement Radiometer Brightness Temperature Data Product. Jet Propulsion Laboratory, California Institute of Technology, pp. 24.
Colliander, A., Jackson, T., Bindlish, R., Chan, S., Das, N., Kim, S., Cosh, M., Dunbar, R., Dang, L., Pashaian, L., 2017. Validation of SMAP surface soil moisture products with core validation sites. Remote Sens. Environ. 191, 215–231.
Crow, W., Bindlish, R., Jackson, T., 2005. The added value of spaceborne passive microwave soil moisture retrievals for forecasting rainfall-runoff partitioning. Geophys. Res. Lett. 32, L18.
Crow, W.T., Berg, A.A., Cosh, M.H., Loew, A., Mohanty, B.P., Panciera, R., de Rosnay, P., Ryu, D., Walker, J.P., 2012. Upscaling sparse ground-based soil moisture observations for the validation of coarse-resolution satellite soil moisture products. Rev. Geophys. 50, RG2002.
Das, N.N., Entekhabi, D., Kim, S., Yueh, S., O'Neill, P., 2016. Combining SMAP and Sentinel data for high-resolution Soil Moisture product. In: 2016 IEEE International Geoscience and Remote Sensing Symposium (IGARSS 2016). IEEE, Beijing, China, pp. 129–131.
de Rosnay, P., Drusch, M., Boone, A., Balsamo, G., Decharme, B., Harris, P., Kerr, Y., Pellarin, T., Polcher, J., Wigneron, J.-P., 2009. AMMA land surface model intercomparison experiment coupled to the community microwave emission model: ALMIP-MEM. J. Geophys. Res. 114, D05108.
Dumedah, G., Walker, J.P., Rudiger, C., 2014. Can SMOS data be used directly on the 15-km discrete global grid? IEEE Trans. Geosci. Remote Sens. 52, 2538–2544.
Entekhabi, D., Asrar, G.R., Betts, A.K., Beven, K.J., Bras, R.L., Duffy, C.J., Dunne, T., Koster, R.D., Lettenmaier, D.P., McLaughlin, D.B., 1999. An agenda for land surface hydrology research and a call for the second international hydrological decade. Bull. Am. Meteorol. Soc. 80, 2043–2058.
Entekhabi, D., Njoku, E.G., O'Neill, P.E., Kellogg, K.H., Crow, W.T., Edelstein, W.N., Entin, J.K., Goodman, S.D., Jackson, T.J., Johnson, J., 2010. The soil moisture active passive (SMAP) mission. Proc. IEEE 98, 704–716.
Entekhabi, D., Das, N., Njoku, E., Yueh, S., Johnson, J., Shi, J., 2014. Algorithm Theoretical Basis Document L2 & L3 Radar/Radiometer Soil Moisture (Active/Passive) Data Products. Jet Propulsion Laboratory, California Institute of Technology, pp. 89.
Falloon, P., Jones, C.D., Ades, M., Paul, K., 2011. Direct soil moisture controls of future global soil carbon changes: an important source of uncertainty. Glob. Biogeochem. Cycles 25, GB3010.
Gevaert, A., Parinussa, R.M., Renzullo, L.J., van Dijk, A.I., de Jeu, R.A., 2016. Spatio-temporal evaluation of resolution enhancement for passive microwave soil moisture and vegetation optical depth. Int. J. Appl. Earth Obs. Geoinf. 45, 235–244.
Jung, M., Reichstein, M., Ciais, P., Seneviratne, S.I., Sheffield, J., Goulden, M.L., Bonan, G., Cescatti, A., Chen, J., De Jeu, R., 2010. Recent decline in the global land evapotranspiration trend due to limited moisture supply. Nature 467, 951–954.
Kerr, Y.H., Waldteufel, P., Wigneron, J.-P., Delwart, S., Cabot, F., Boutin, J., Escorihuela, M.J., Font, J., Reul, N., Gruhier, C., 2010. The SMOS Mission: new tool for monitoring key elements ofthe global water cycle. Proc. IEEE 98, 666–687.
Liu, J., 2000. Smoothing filter-based intensity modulation: a spectral preserve image fusion technique for improving spatial details. Int. J. Remote Sens. 21, 3461–3472.
Mo, T., Choudhury, B.J., Schmugge, T.J., Wang, J.R., Jackson, T.J., 1982. A model for microwave emission from vegetation-covered fields. J. Geophys. Res. 87 (11229-11211,11237).
Moran, P.A., 1950. Notes on continuous stochastic phenomena. Biometrika 37, 17–23.
Panciera, R., Walker, J.P., Jackson, T.J., Ryu, D., Gray, D., Monerris, A., Yardley, H., Tanase, M.A., Rüdiger, C., Wu, X., Gao, Y., H., J., 2014. The soil moisture active passive experiments (SMAPEx): towards soil moisture retrieval from the SMAP Mission. IEEE Trans. Geosci. Remote Sens. 52, 490–507.
Peng, J., Loew, A., Merlin, O., Verhoest, N.E., 2017. A review of spatial downscaling of satellite remotely sensed soil moisture. Rev. Geophys. 55, 341–366.
Rüdiger, C., Su, C.-H., Ryu, D., Wagner, W., 2016. Disaggregation of low-resolution l-band radiometry using c-band radar data. IEEE Geosci. Remote Sens. Lett. 13, 1425–1429.
Ryu, D., Famiglietti, J.S., 2006. Multi-scale spatial correlation and scaling behavior of surface soil moisture. Geophys. Res. Lett. 33, L08404.
Sabaghy, S., Walker, J.P., Renzullo, L.J., Jackson, T.J., 2018. Spatially enhanced passive microwave derived soil moisture: capabilities and opportunities. Remote Sens. Environ. 209, 551–580.
Sellers, P.J., Dickinson, R.E., Randall, D.A., Betts, A.K., Hall, F.G., Berry, J.A., Collatz, G.J., Denning, A.S., Mooney, H.A., Nobre, C.A., 1997. Modeling the exchanges of energy, water, and carbon between continents and the atmosphere. Science 275, 502–509.
Seneviratne, S.I., Corti, T., Davin, E.L., Hirschi, M., Jaeger, E.B., Lehner, I., Orlowsky, B., Teuling, A.J., 2010. Investigating soil moisture–climate interactions in a changing climate: a review. Earth Sci. Rev. 99, 125–161.
Torres, R., Snoeij, P., Geudtner, D., Bibby, D., Davidson, M., Attema, E., Potin, P., Rommen, B., Floury, N., Brown, M., 2012. GMES Sentinel-1 mission. Remote Sens. Environ. 120, 9–24.
Ulaby, F.T., Moore, R.K., Fung, A.K., 1981. Microwave Remote Sensing: Active and Passive. Volume I-Microwave Remote Sensing Fundamentals and Radiometry. Artech House, Boston, MA.
Wigneron, J.-P., Kerr, Y.H., Waldteufel, P., Saleh, K., Escorihuela, M.J., Richaume, P., Ferrazzoli, P., De Rosnay, P., Gurney, R., Calvet, J.C., 2007. L-band microwave emission of the biosphere (L-MEB) model: description and calibration against experimental data sets over crop fields. Remote Sens. Environ. 107, 639–655.
Ye, N., Walker, J.P., Rüdiger, C., 2015. A cumulative distribution function method for normalizing variable-angle microwave observations. IEEE Trans. Geosci. Remote Sens. 53, 3906–3916.
Ye, N., Walker, J.P., Wu, X., Jeu, R.d., Gao, Y., Jackson, T.J., Jonard, F., Kim, E., Merlin, O., Pauwels, V., Renzullo, L., Rüdiger, C., Sabaghy, S., Hebel, C.v., Yueh, S.H., Zhu, L., 2018. The soil moisture active passive experiments: towards calibration and validation of the SMAP mission. Remote Sens. Environ (submitted).